Journal of Cleaner Production 284 (2021) 124757

Contents lists available at ScienceDirect

Journal of Cleaner Production

journal homepage: www.elsevier.com/locate/jclepro

Ultra-fast and highly efficient hybrid material removes Cu(II) from wastewater: Kinetic study and mechanism

Mohamed El-Massaoudi [a], Smaail Radi [a, **], Morad Lamsayah [a], Said Tighadouini [b], Konan Kouakou Séraphin [c], Lazare Kouakou Kouassi [c], Yann Garcia [d, *]

[a] Laboratory of Applied and Environmental Chemistry (LCAE), Faculté des Sciences, Université Mohamed Premier, 60 000, Oujda, Morocco
[b] Laboratoire de Synthèse Organique, Extraction et Valorisation, Faculté des Sciences Aïn-Chock, Université Hassan II Casablanca, 20100, Morocco
[c] Laboratory of Environmental Science and Technology, Université Jean Lorougnon Guédé, BP V 25, Daloa, Cote d'Ivoire
[d] Institute of Condensed Matter and Nanosciences, Molecular Chemistry, Materials and Catalysis (IMCN/MOST), Université Catholique de Louvain, Place Louis Pasteur 1, 1348, Louvain-la-Neuve, Belgium

ARTICLE INFO

Article history:
Received 29 June 2020
Received in revised form
13 October 2020
Accepted 18 October 2020
Available online 21 October 2020

Handling Editor. Prof. Jiri Jaromir Klemeš

Keywords:
Water cleaning technologies
Hybrid materials
Real water samples analysis
Copper(II)
Heavy metals
Depollution

ABSTRACT

Water pollution by toxic elements represents a significant risk to the environment and human ecosystem, and a number of efforts are developed to find a suitable solution. In this work, a new adsorbent based on silica gel as an inert material modified on surface by a pincer ligand was prepared. The hybrid material has been synthesized via a simple Schiff base reaction and characterized by several relevant physical methods. The adsorbent shows an extremely rapid efficiency in removal of copper (less than 8 min) with maximum sorption capacity of 1.90 mmol g^{-1} and a rapid efficiency for zinc, cadmium and lead (less than 20 min) with adsorption capacities 0.52, 0.49 and 0.43 mmol g^{-1}, respectively. A kinetic study shows that the sorption can be described by a pseudo second-order model, and that the process is thermodynamically spontaneous and endothermic. The adsorbent shows a high selectivity to Cu(II) and a great reusability after five adsorption-desorption cycles. Theoretical, energy dispersive X-ray fluorescence (EDX) and Fourier transform-infrared spectroscopy studies demonstrate that the uptake occurs by a coordination reaction between metal ions and the pincer ligand on the surface of the adsorbent. The efficiency of this new hybrid material was confirmed in removal of Cu(II) from real water samples originating from Abidjan Atlantic sea bay, one of the most polluted region in West Africa, as well as from rivers located near Oujda, Morocco.

1. Introduction

Heavy metal ions originating from industrial waste represent a real threat and even a danger to the whole ecosystem (Azimi et al., 2017). Indeed, the dumping of these metals in rivers or even in the oceans is very harmful to all living beings and aquatic environment which are not immune from the scourge of their irreversible effects. High concentrations of these metals are also toxic to plants, animals and living organisms (Abbas et al., 2014; Burakov et al., 2018).

The harmful effect of heavy metals is due to their ability to easily bind to organic elements that make up the atmosphere, in particular, oxygen, nitrogen and even sulphur. These elements, which are also found in proteins, easily lead to alterations in enzyme activity (Sarwar et al., 2017). The toxicity of heavy metals to living beings varies with the metal involved, the extent of exposure, the duration of contamination, the age of the individual and chronicity (Rehman et al., 2018). It is therefore timely to protect the environment by applying regulations signed at recognized international conventions. Scientists are constantly reminding about the importance of maintaining the balance of mineral elements in nature, but their discharge into rivers is to regret very harmful to the ecosystem (Bu et al., 2019; Vojoudi et al., 2018). For example, copper is a micro-essential trace element which plays an important role in the development of physiological processes of human beings and other living organisms (Barrento et al., 2008). Like any micronutrient, copper is essential at very low concentrations, but it quickly becomes toxic at high concentrations causing various health issues, especially damage to the liver, bones and the central

* Corresponding author.
** Corresponding author.
E-mail addresses: s.radi@ump.ac.ma (S. Radi), yann.garcia@uclouvain.be (Y. Garcia).

https://doi.org/10.1016/j.jclepro.2020.124757
0959-6526/

nervous system, if not the entire immune system (Wondracek et al., 2016).

So far, several methods have been deployed to treat heavy metals from wastewater, such as chemical precipitation and membranes (Abdu et al., 2014; Das et al., 2014), but these have many drawbacks, including high economic and energy costs, low disposal efficiency, regeneration and the generation of large quantities of chemical waste (Al-Saydeh et al., 2017).

Currently, surface adsorption has been identified as the most promising technology for the removal of pollutants from wastewater, due to its simplicity of operation, regeneration of adsorbents and low cost (Gandavadi et al., 2019; Nabeela et al., 2019). Among adsorbents, inexpensive silica gel-based adsorbents for the cleanup and purification of wastewater have also been described (Fu et al., 2019; Radi et al., 2019). This class of porous materials has rapidly risen to the forefront of materials research because of their internal surfaces, easy chemical bonding, and extraordinary ability to selectively adsorb large quantities of guest species (Awual, 2017; Radi et al., 2017). The potential for silica gel to be used in water purification is related to the ease with which their internal surfaces can be decorated by functionalization offering important densities of adsorption sites (Tighadouini et al., 2020).

Silica gel is routinely modified by surface modification (Bai et al., 2019; Zhang, W. et al., 2019). Among SiO_2, $SiO-NH_2$ amine could be effectively modified to incorporate various functional groups on the surface since the amino groups can be functionalized easily (Isasi et al., 2019; Sosa et al., 2020). It has been reported too that amino groups on silica gel can be covalently modified by several reagents such as acetic acid (Rasheed et al., 2020), Schiff bases (Radi et al., 2016b; Xu et al., 2018; Zhao et al., 2020), ketoenols (Tighadouini et al., 2017, 2018'bib_Tighadouini_et_al_2018'bib_Tighadouini_et_al_2017), amino acids (Petrova et al., 2017), ionic liquids (Barik et al., 2020), and dendrimers (Song et al., 2017; Zhang et al., 2018). These results demonstrate the importance to prepare and apply a silica gel-based ligand as an absorbent for the capture of Cu(II), Cd(II), Zn(II) and Pb(II) ions due to its chelating power.

The goal of this work is the preparation of an adsorbent with a high adsorption capacity and high selectivity towards a metal ion. The choice of pyridine-2,6-dicarbaldehyde (**PyO**) for fixation on the surface of ***SiNH$_2$*** is justified by the complexing ability of pyridine towards metal ions. In this case, the 3-aminotrimethoxysile will act as a spacer arm to facilitate the flexibility of the grafted ligand on the surface of silica gel. In addition, the condensation of the amino groups with **PyO** will create a pincer ligand NNN sp^2 on the surface of silica gel, which has enormous complexing power (Römelt et al., 2019). The successful modification of silica gel was confirmed by several characterization methods. Experimental parameters that affect the adsorption capacity such as: pH of the solution, adsorption time, effect of temperature and concentration of the complexed agent have been studied. In addition, the experimental data have been fitted with different models, not only to quantify the adsorption performance, but also to interpret the adsorption processes of the ***SiNNN*** adsorbent. To better understand the adsorption behaviour of the new adsorbent, DFT was used to predict the structure of the complex formed on the surface of the material. The high adsorption capacity and the selectivity linked to the quickness of catching copper from wastewater constitute the main assets of this new adsorbent.

2. Experimental section

This section contains the chemicals and materials used, as well as describes the methods for ligand and material synthesis, and the adsorption methodology used.

2.1. Materials

All solvents and chemicals (Sigma-Aldrich, purity > 99.5%) were of analytical grade and used without further purification. Silica gel (E. Merck) with a median pore diameter of 60 Å and a range 70−230 mesh range for the particle size was used. Spectra Varian A.A. 400 spectrophotometer was used for atomic absorption measurements. Elemental analyses were performed by the Microanalysis Centre Service at Vernaison, France (CNRS). FT-IR spectra were obtained using a PerkinElmer System 2000. SEM images were obtained on an FEI-Quanta 200. Thermogravimetric measurements were performed by a PerkinElmer Diamond TG/DTA. CP MAX CXP 300 MHz instrument was used to obtain the solid state ^{13}C NMR spectrum. Surface area and pore volume size were obtained by a Thermoquest Sorpsomatic 1990 analyzer. Energy dispersive X-ray fluorescence (EDX) data were registered on a Shimadzu EDX 7000.

2.2. Methods

2.2.1. Synthesis of $SiNH_2$ and SiNNN

The preparation of pyridine-2,6-dicarbaldehyde, amino silica gel ***SiNH$_2$*** and ***SiNNN*** is described in Scheme 1. Firstly, pyridine-2,6-dicarbaldehyde was prepared by reacting pyridine-2,6-diyldimethanol (3 g) with activated MnO_2 (12 g) in presence of chloroform (50 mL) as solvent. The mixture was refluxed with stirring for 24 h. Then, MnO_2 was filtered and washed many times with hot chloroform and methanol. The solvent was removed under pressure to yield to pyridine-2,6-dicarbaldehyde (**PyO**). Yield: 65% (1.89 g). ^1H NMR (300 MHz, DMSO) δ ppm: 10.12 (2H, aldehyde), 8.33 and 8.23 (3H, pyridine).

In a second step, 3-aminotrimethoxysilane was mixed with free silica gel activated by heating at 120 °C for 24 h to obtain **SiNH$_2$** following the method developed recently (El-Massaoudi et al., 2018; Radi et al., 2017). Thirdly, **SiNH$_2$** (5 g) was reacted with **PyO** (2 g) in reflux of methanol (50 mL) for 24 h. The orange hybrid material formed was filtered, dried and then Soxhlet extracted using methanol and dichloromethane (1/1) for 12 h. The ***SiNNN*** was then dried under vacuum at 60 °C over 24 h.

2.2.2. Adsorption studies

The adsorption of metal ions on ***SiNNN*** was performed in a batch experiment. All adsorption tests were carried out in triplicate for each sample and only the mean data were reported. After adsorption, the solid phase was then separated by filtration using a 0.45 μm syringe filter. The residual concentration of metal ion in the filtrate was measured by an atomic absorption spectrophotometer.

The adsorption capacity of the cations was calculated using Eq. (1):

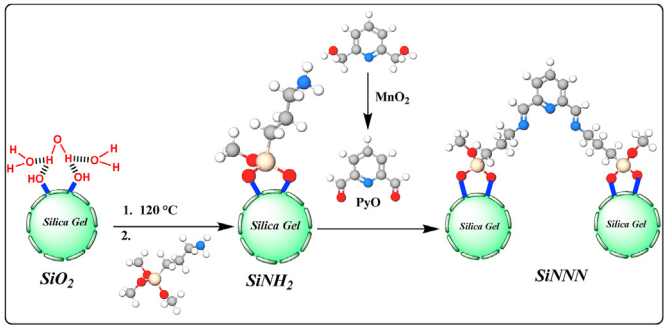

Scheme 1. Elaboration of hybrid materials ***SiNH$_2$*** and ***SiNNN.***

$$q_e = (C_0 - C_e) \times \frac{V}{m} \quad (1)$$

where q_e is the amount of metal ions on the adsorbent (mmol g^{-1}), V is the volume of metallic solution (L), m is the weight of ***SiNNN*** (g), C_0 is the initial concentration of metal ions (mmol L^{-1}), and C_e is the equilibrium metal ion concentration in solution (mmol L^{-1}).

pH **studies.** ***SiNNN*** (10 mg) was added into a conical flask containing solution at optimum concentrations of metal ions. The mixture was adjusted to a suitable pH with a solution of HCl and NaOH. Then, the adsorption experiments were carried out at an initial pH between 2.0 and 7.0 and 180 mg L^{-1} at 298 K in 30 min.

Temperature studies: The adsorbent ***SiNNN*** (10 mg) in metal solutions (10 mL, pH 6.0 and 180 mg L^{-1}) was used to perform a test of the effect of temperature (298, 308 and 318 K) for 30 min.

Effect of Contact Time. Experimental tests on effects of shaken time (5, 10, 15, 20, 25, 30 and 35 min) were performed using ***SiNNN*** (10 mg) in metal solutions (10 mL) of 180 mg L^{-1} of each metal ion, at 298 K and pH = 6.0.

Adsorption in a mixture of metal solution. A mixture of metal solutions (pH 6.0, optimum concentration of each) were prepared, with $Cu(NO_3)_2{\bullet}3H_2O$, $Zn(NO_3)_2{\bullet}6H_2O$ $Cd(NO_3)_2{\bullet}6H_2O$ and $Pb(NO_3)_2{\bullet}6H_2O$. The experiment was performed by placing the ***SiNNN*** adsorbent (10 mg) in a conical flask containing a mixture of metal solutions (10 mL) at 298 K for 30 min.

Adsorption mechanism: DFT calculations. The geometry of the ligand decorating the surface of silica gel has been optimized at the level of a B3LYP/6-31G (d,p) calculation using the Gaussian program 09 (Becke, 1992; Frisch et al., 2009; Lee et al., 1988). Multiwfn, VMD and GaussView Softwares (Lu, 2014; Roy and Millam, 2009) were used to calculate and visualize the molecular electrostatic potential properties (MESP).

3. Results and discussion

Material characterization, adsorption study and its mechanism are discussed in this section.

3.1. Characterisation of functionalized SiNNN

The modification of silica gel to get the hybrid material was tracked using Fourier transform-infrared spectroscopy (FTIR), elemental analysis, solid state ^{13}C NMR, thermogravimetry analysis (TG), scanning electron microscopy (SEM) and surface area and pore volume size analysis (nitrogen adsorption–desorption isotherm, BET surface area, BJH pore volume size). The outcome of these analysis is described below.

3.1.1. FTIR

FTIR plots for functionalized silica gel ***SiNH$_2$*** and ***SiNNN*** are presented in Fig. 1. Both spectra show repetitive behaviour in the bands: 3459 and 3487 cm^{-1}, 2951 and 2945 cm^{-1}, and 802 cm^{-1}, assigned to O–H, stretching C–H, bend Si–OH and C–C vibrations, respectively (El Abiad et al., 2019). Additionally, 1652 cm^{-1}, 1097 $cm^{-1}$and 468 cm^{-1} were assigned to silica vibration bands such as Si–OH bend, Si–O–Si and Si–O (Radi et al., 2018). In the spectrum of ***SiNH$_2$***, the peak at 1560 cm^{-1} was attributed to N–H bending (Radi et al., 2016a). At the time of grafting organic ligands onto ***SiNH$_2$***, in the spectrum FT-IR of ***SiNNN*** new peaks have been observed. The new bands arising at 1654 cm^{-1} and 1448 cm^{-1} correspond to C=N and C=C vibrations belonging to organic ligands. Consequently, the resulting ***SiNNN*** spectrum clearly demonstrates the successful binding of the ligand to the silica surface.

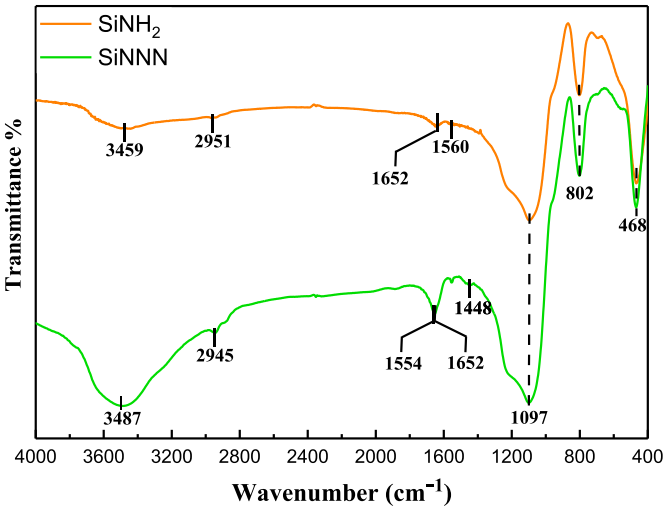

Fig. 1. FTIR spectra of functionalized silica gels ***SiNH$_2$*** and ***SiNNN***.

3.1.2. Elemental analysis

The elemental analysis was used to determine the presence and modification in the elemental composition of the materials. As shown in Table 1, the N content of the ***SiNH$_2$*** material was slightly lower than that of the ***SiNNN*** material as expected with the introduction of ***PyO*** on ***SiNH$_2$*** whereas the C content is almost doubled. The C/N ratio of ***SiNNN*** is much higher than the one of ***SiNH$_2$***, due to the ***PyO*** grafting which contains many C and N atoms. The successful synthesis of ***SiNNN*** was confirmed.

3.1.3. ^{13}C NMR analyses

^{13}C NMR spectroscopy is the most efficient method currently available to examine the chemical structures of carbon materials. The ^{13}C NMR spectrum of the ***SiNNN*** material, shown in Fig. 2, clearly allows to distinguish the peaks of the pyridine ring at 135.18 ppm for carbon in para position, 120.79 ppm for meta carbon

Table 1
Elemental analysis in percent (%) of carbon, nitrogen and C/N ratio for the hybrid materials ***SiNH$_2$*** and ***SiNNN***.

Simple	Elemental Analysis		
	C (%)	N (%)	C/N ratio
SiNH$_2$	4.46 (6)	1.66 (2)	2.68
SiNNN	8.89 (3)	1.77 (4)	5.02

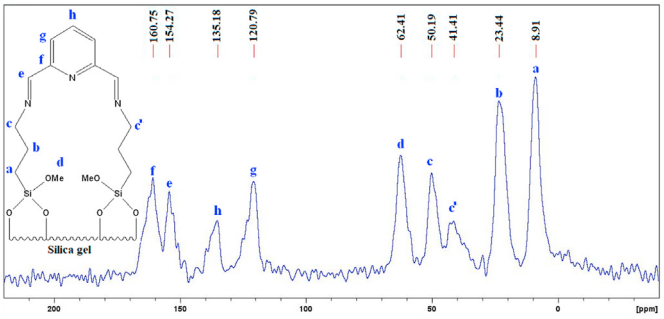

Fig. 2. Solid-state ^{13}C NMR spectrum of ***SiNNN*** (CPMAS R_0 = 12.5 Hz, 4 mm standard probe).

and 160.75 ppm for ortho pyridine. In addition, the carbon signal bound to the group imine is observed at 154.27 ppm, in agreement with the reaction of the amine with ***PyO*** dialdehyde. The 62.41 ppm signal was assigned to the methoxy group not bounded to the silica gel surface, as well as the (50.19 ppm, 41.41 ppm), 23.44 ppm and 8.91 ppm signals assigned to the **C**–N, C–**C**–C and **C**–Si groups, respectively, belonging to the propyl amino spacer between the ***PyO*** ligand and the silica gel.

These results suggest that the amino group hydrogens on the **SiNH$_2$** surface have been substituted by pyridine dialdehyde by Schiff base reaction. This means that the ***SiNNN*** absorbent has been successfully synthesized by chemical modification of the surface.

3.1.4. TG analyses

Thermogravimetric analyses (TG) were used to assess the thermal stability of the materials in the temperature range of 30–800 °C. The thermogram of ***SiNH$_2$*** reveals two decomposition steps (Fig. 3a): a first one with 2.01% weight loss at temperatures between 25 and 200 °C as a result of moisture evaporation such as adsorbed water and organic solvents; and a second one with 7.7%, from 200 to 800 °C, attributed to the thermal degradation of the organic building block 3-aminopropyl from 200 to 500 °C and the condensation of silanol groups (500–800 °C) (Tighadouini et al., 2019). Most notably, two decomposition steps have been observed in the profile of the ***SiNNN*** material (Fig. 3b). In the first stage, 2.14% of the weight loss was due to moisture and the removal of volatile impurities. For the second stage, a very significant weight loss of 12.98%, was attributed to the decomposition of both the spacer group (3-animopropyl) and the pyridine group of the ***SiNNN*** material (200–500 °C), as well as to the condensation of free silanol groups (500–800 °C). In addition, the material ***SiNNN*** shows a good thermostability, which means that the material can remain stable even at high temperatures (>200 °C).

3.1.5. Morphology of the surface

SEM images of the samples are illustrated in Fig. 4, where the morphology and surface structure of each sample is represented. Under the microscope, the SEM image of free silica ***SiO$_2$*** reveals smoother and more homogeneous surfaces than those of ***SiNH$_2$*** and ***SiNNN***. Indeed, compared to ***SiO$_2$*** silica gel, ***SiNH$_2$*** and ***SiNNN*** materials had coarse surfaces with protuberances and valleys (Fig. 4). These changes are mainly related to transplantation in the first step of 3-aminotrimothoxysilane (***SiNH$_2$***) and in the second step, to the reaction of ***PyO*** with ***SiNH$_2$*** (***SiNNN***). In addition, ***SiNNN*** appears as a porous and rough adsorbent, which has been attributed to cavities that have been formed on its surface. More importantly, the pleated and porous surfaces that increased adsorption sites could be beneficial for coordination between functional groups **NNN** and metal ions.

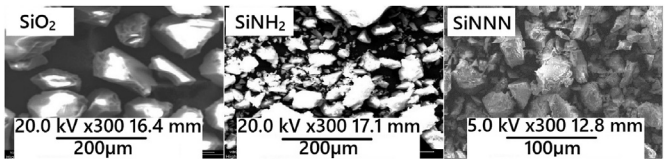

Fig. 4. SEM images of free silica (***SiO$_2$***), amino silica (***SiNH$_2$***) and adsorbent (***SiNNN***).

3.1.6. Surface area and pore volume size analysis

The BET and BJH have been applicated on the samples ***SiNH$_2$*** and ***SiNNN*** to determine the specific area ($m^2\ g^{-1}$) and pore volume ($cm^3\ g^{-1}$) (Fig. 5). The values of the S_{BET} (305.21 $m^2\ g^{-1}$) and the pore volume (0.77 $cm^3\ g^{-1}$) of ***SiO$_2$*** (Tighadouini et al., 2020) decrease when the surface is modified by 3-aminopropyltrimethoxysilane to get ***SiNH$_2$*** (S_{BET} = 283.08 $m^2\ g^{-1}$ and V_{pore} = 0.69 $cm^3\ g^{-1}$). For ***SiNNN*** (S_{BET} = 343.66 $m^2\ g^{-1}$ and V_{pore} = 0.44 $cm^3\ g^{-1}$), the pore volume and the average pore diameter have been decreased, except the specific surface which increase from 238.08 to 343.66 $m^2\ g^{-1}$, which can be explained by the increase of pore numbers, that can be considered as a suitable material for bonding metal ions.

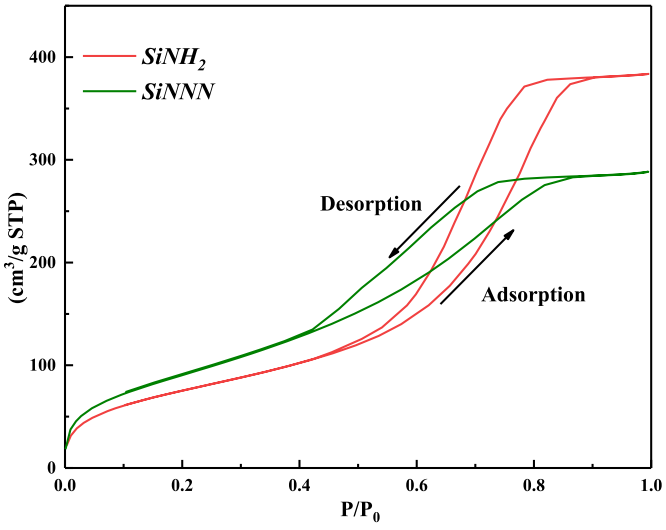

Fig. 5. Nitrogen adsorption–desorption isotherm of ***SiNH$_2$*** and ***SiNNN***.

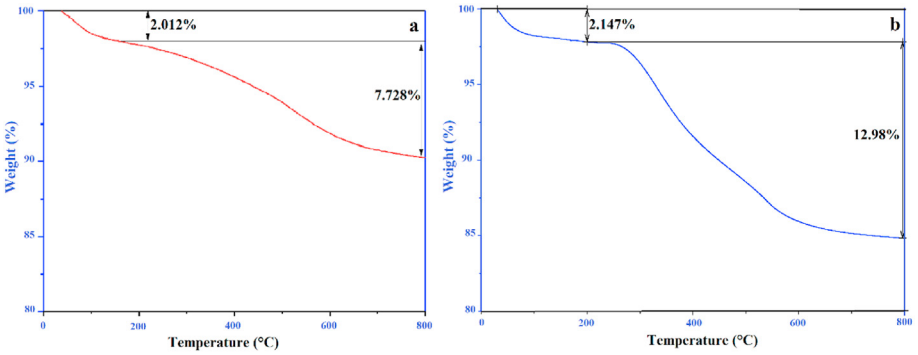

Fig. 3. Thermograms of ***SiNH$_2$*** (a) and the adsorbent ***SiNNN*** (b).

3.2. Adsorption characteristics of SiNNN

The adsorption on the material ***SiNNN*** are studied and analyzed under various conditions within this section.

3.2.1. Effect of pH

The effect of pH was investigated due to its importance in the evolution of the adsorption performance of heavy metal ions on ***SiNNN*** adsorbent (Fig. 6). A gradual increase in the adsorption capacity of the adsorbent with increasing pH was observed. The maximum adsorption capacity of the metal ions was obtained at pH = 6. In acid aqueous solution, there is a very large amount of hydronium ions H_3O^+, which compete with metal ions to engage with the adsorption sites available on the surface of the adsorbent (The three nitrogen sp^2 atoms of the ligand). Whenever the pH value was increased, the concentration of H_3O^+ ions was reduced, it means that the competition of H_3O^+ with the metal ion decreases, the adsorption capacity of the metal ions increases caused by electrostatic attractive between active groups and cationic metals.

3.2.2. Adsorption kinetics

Adsorption rate is one of the crucial factors in assessing the applicability of an adsorbent. In this study, the experimental contact time data shown in Fig. 7.a reveals a super-fast adsorption of Cu(II) of only 8 min to achieve maximum sorption capacity. This adsorption velocity can be explained by the availability of hydrophilic groups on the adsorbent's surface. On the other hand, for Pb(II), Zn(II) and Cd(II) the saturation was reached after 20 min (Fig. 7b). Consequently, the reason for the higher velocity of ***SiNNN*** for Cu(II) could be that the Cu(II) ion has a stronger attraction to the hydrophilic nitrogen electrons of the pincer ligand on the surface.

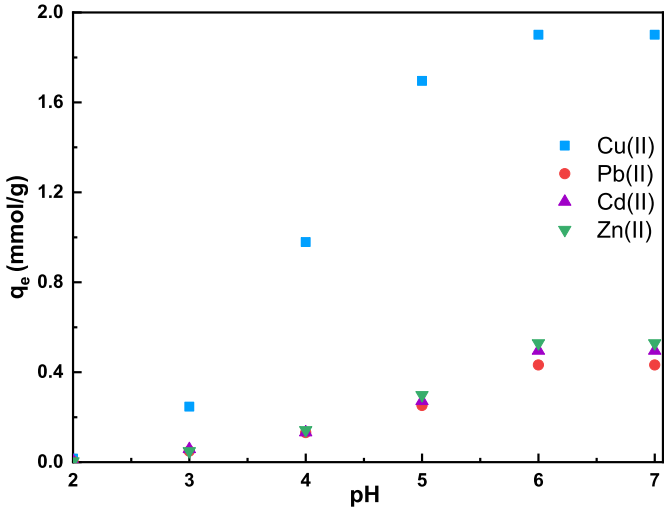

Fig. 6. Effect of pH on adsorption of metals using ***SiNNN***, conditions (V = 10 mL metal solutions, m = 10 mg of adsorbent, C_0 = 180 mg L^{-1}, t = 30 min, T = 25 °C).

Two models, namely pseudo-first order (PFO) and pseudo-second order (PSO), have been applied to investigate the kinetic mechanism involved in the adsorption process (Guo and Wang, 2019; Moussout et al., 2018). The experimental data were fitted according to Eq. (2) and Eq. (3) for PFO and PSO, respectively (de la Luz-Asunción et al., 2019; Gusain et al., 2016):

$$q_t = q_e\left[1 - e^{-k_1 t}\right] \tag{2}$$

$$q_t = \frac{k_2 q_e^2 t}{1 + k_2 q_e t} \tag{3}$$

where q_t and q_e are the adsorption capacity of metal ions (mmol g^{-1}) time t and at equilibrium, respectively; K_1 (min^{-1}) and K_2 (g mol^{-1} min^{-1}) are the rate constant of the PFO and PSO, respectively. The kinetic parameters are listed in Table 2.

The best correlation coefficients (R^2) were obtained for the PSO model which points out to a chemical interaction between solute and the surface of adsorbent. The PSO model suggests that solute adsorption (metal ions) is proportional to the active sites available on the adsorbent surface (***SiNNN***). The great dispersion of the ligand on the inorganic surface may favour a chemical interaction between the hydrophilic nitrogen and metal ions.

3.2.3. Thermodynamic study

Temperature has a notable effect on the ability of adsorbents to remove trace elements. As shown in Fig. 8.a, the potentially toxic elements removal performance emerges as a remarkable efficiency of the adsorbent with increasing temperature. In order to prove the thermodynamic characteristic of the adsorption process between the adsorbate (metal ions) and the adsorbent (***SiNNN***), the thermodynamic parameters including enthalpy (ΔH), entropy (ΔS) and Gibbs free energy (ΔG) were calculated by Van't Hoff diagrams using the following equations (4)–(6) (Salvestrini et al., 2014; Zhou and Zhou, 2014):

$$K = K_d \times 10^3 \times \gamma \tag{4}$$

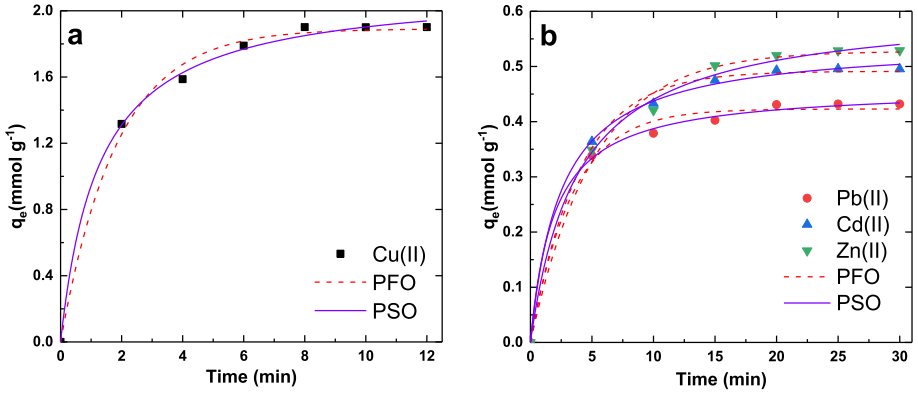

Fig. 7. Effect of time on Cu(II) (a) and Zn(II), Cd(II) and Pb(II) (b) adsorption onto ***SiNNN***. Nonlinear PFO and PSO kinetic models fits. Conditions (V = 10 mL metal solutions, m = 10 mg of adsorbent, C_0 = 180 mg L^{-1}, pH = 6, t = 30 min, T = 25 °C).

Table 2
Kinetic parameters using pseudo-first order (PFO) and pseudo-first order (PSO) models for adsorption of metal ions into ***SiNNN.***

Adsorbent	Metal ions	q_e (exp) (mmol g^{-1})	PFO			PSO		
			K_1 (min^{-1})	q_e (mmol g^{-1})	R^2	K_2 (g mol^{-1} min^{-1})	q_e (mmol g^{-1})	R^2
SiNNN	Cu(II)	1.90 ± 0.0004	0.54 ± 0.04	1.89 ± 0.03	0.994	0.36 ± 0.04	2.14 ± 0.03	0.997
	Zn(II)	0.52 ± 0.0004	0.19 ± 0.01	0.52 ± 0.01	0.993	0.42 ± 0.06	0.61 ± 0.01	0.998
	Cd(II)	0.49 ± 0.0002	0.25 ± 0.01	0.49 ± 0.01	0.996	0.74 ± 0.06	0.54 ± 0.01	0.999
	Pb(II)	0.43 ± 0.0001	0.29 ± 0.03	0.42 ± 0.01	0.992	1.12 ± 0.13	0.46 ± 0.01	0.998

$$\Delta G = -RT\,Ln\,K \tag{5}$$

$$Ln\,K = -\frac{\Delta H}{RT} + \frac{\Delta S}{R} \tag{6}$$

K_d is the experimental distribution constant, K is the equilibrium constant, γ is the coefficient of activity, R (8.314 J mol^{-1} K^{-1}) is the ideal gas constant, ΔG (kJ mol^{-1}) is the Gibbs free energy change of the system, ΔH (kJ mol^{-1}) is the enthalpy change of the system, ΔS (J K^{-1} mol^{-1}) is the entropy change of the system, and T (K) is the temperature.

The parameters ΔH, ΔS and ΔG summarized in Table 3 were calculated using the plot of ln K vs $1/T$ (Fig. 8b). An endothermic sorption nature can be observed by the positive value of enthalpy

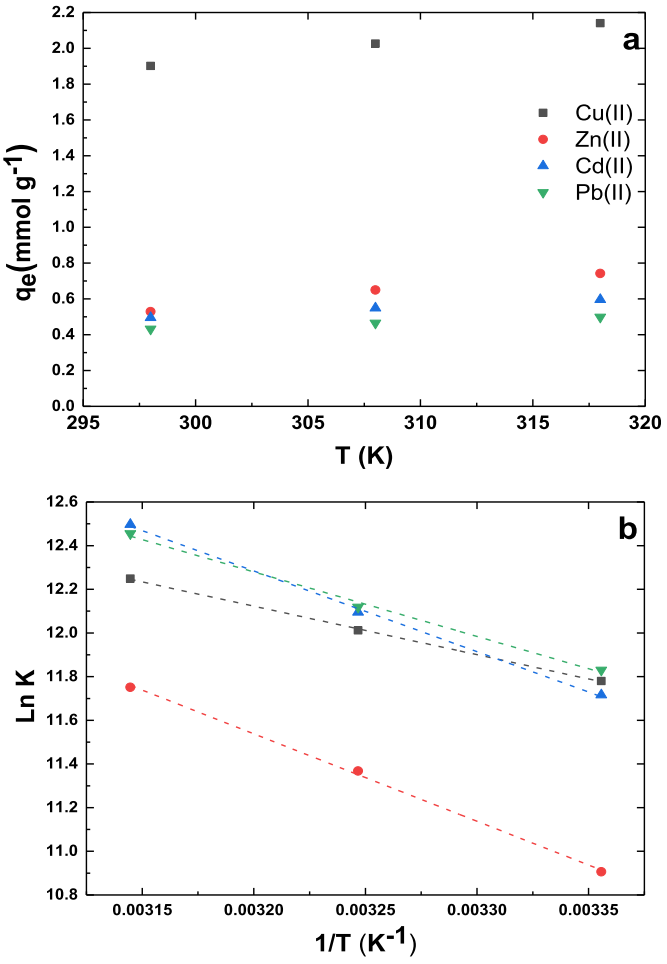

Fig. 8. Effect of temperature on adsorption of metal ions onto ***SiNNN*** (a), linear plots of equilibrium constant K *vs.* $1/T$ (b). (Conditions: V = 10 mL metal solutions, m = 10 mg of adsorbent, C_0 = 180 mg L^{-1}, pH = 6, t = 30 min, T = 25, 35 and 45 °C).

$\Delta H > 0$, that explain the increase of adsorption capacities with increasing of temperature for all metal ions (Fig. 8a). An increasing in the randomness at the interface adsorbate/adsorbent is confirmed by the positive value $\Delta S > 0$. The negative value $\Delta G < 0$ indicated that the adsorption reaction was spontaneous and feasible at 298 K and the decrease value of ΔG with increase of temperature stipulates that the adsorption of heavy metals was more favorable at higher temperature and the active sites on the surface of ***SiNNN*** become more accessible. In addition, ΔG values below 40 kJ mol^{-1} involve that the adsorption exhibits some chemisorption (Chen et al., 2019).

3.2.4. Effect of mixture of heavy metals

One of the most important factors for the practical application of an adsorbent for the treatment of real water is the selective removal of a heavy metal from a mixture of metal ions. The selectivity of metal removal has been investigated based on the competition between metal ions during adsorption processes. In this case, the active adsorption sites is known to be selective according to physico-chemical parameters such as electronegativity, ionic radius, charge, electrostatic attraction, etc … (Khandaker et al., 2020).

The adsorption efficiency of an ion in the presence of various competitive ions (Cu(II), Zn(II), Cd(II) and Pb(II)) was studied using a solution containing all four metal ions with a concentration of 180 mg L^{-1} for each ion. The results displayed in Fig. 9.a reveal that the strong ability of the pincer ligand on the surface of silica gel to uptake Cu(II) over other ions. The adsorbent **SiNNN** shows a high suitability and potential applicability for Cu(II) removal from aqueous solutions.

3.2.5. Regeneration and reuse of SiNNN

From an economic point of view, the stability and reusability of any adsorbent are significant factors. For that, the hybrid material ***SiNNN*** has been evaluated by continuous adsorption-desorption cycles (Fig. 9b). The copper ion adsorbed by the ***SiNNN*** was regenerated with 4% HNO_3 as follows: the adsorbent after the adsorption experiment was stirred with 5 mL acid solution for 5 min. The solid was rinsed with 3 × 10 mL distilled water and dried. The regenerated ***SiNNN*** was used in five sequential cycles of experiments. The adsorption efficiencies of Cu(II) on ***SiNNN*** was found to be very stable even after five cycles. As a result, the material can be easy regenerated, has a good stability, and for economic consideration is cheaper.

3.2.6. Adsorption mechanism

DFT calculations. The electrostatic molecular potential (MESP) is related to the electron density. It is a very useful descriptor for determining sites of electrophilic and nucleophilic attack as well as non-covalent interactions (Luque et al., 2000; Okulik and Jubert, 2005; Scrocco and Tomasi, 1979). The blue and red surfaces (3D) covering the molecular structure designate the positive and negative electrostatic potential, respectively. Small red and yellow spheres represent the positions of the local minima and maxima of

Table 3
Thermodynamic parameters for metal ions sorption on ***SiNNN***.

Material	Metal ions	ΔH (kJ mol^{-1})	ΔS (Jk^{-1} mol^{-1})	ΔG (kJ mol^{-1})			R^2
				298 K	308 K	318 K	
SiNNN	Cu(II)	18.478	159.919	−29.177	−30.776	−32.375	0.999
	Zn(II)	33.310	202.520	−27.040	−29.065	−31.090	0.998
	Cd(II)	30.738	200.492	−29.008	−31.013	−33.017	0.998
	Pb(II)	24.577	180.746	−29.284	−31.092	−32.899	0.996

MESP, respectively.

By analysing these minima and maxima, we notice on the surface of ligand on silica gel an overall minimum of −65.47 kcal/mol which is a favorable site for nucleophilic attacks. Its large negative value is due to its characteristic position located at 1.94 Å, 2.28 Å and 2.31 Å from the three nitrogen of the ligand (Fig. 10). All the other minima are enough weak to have attracted the electrostatic potential to it. The global maximum is located along the phenylic group with the greatest value of 20.60 kcal/mol. All the other minimum and maximum point values are usually quite low to have an influence on the reactivity of these ligands. According to this analysis, the complexation involves Metal-Nitrogen coordination bonds of about 1.94 Å, 2.28 Å and 2.31 Å with an interaction energy of −65,47 kcal/mol. Such bond lengths nicely fit with the reported Cu−N ~1.942−2.229 Å by (Weitzer and Brooker, 2005) and (Ghosh et al., 2015) with Cu−N ~ 1.968−2.134 Å for Cu(II) complexes with almost similar ligand. These results show clearly that the metal ions are complexed by the cavity of the NNN pincer ligand.

Energy dispersive X-ray fluorescence (EDX). Additionally, the silica gel surface decorated by the organic ***SiNNN*** ligand before and after adsorption of Cu(II) has been characterized with the energy dispersive X-ray fluorescence (EDX) technique. The EDX spectra in Fig. 11.b clearly shows that the adsorption of the Cu(II) ions was well performed with 12% on the surface of the ***SiNNN*** adsorbent after adsorption compared to ***SiNNN*** before adsorption in Fig. 11.a.

3.2.7. Removal of heavy metal in real wastewater samples

In order to exploit the adsorbent in the removal of trace elements, two natural samples were collected from a polluted environment. Focus was made on the Ebrié lagoon water collected at Cocody Bay in Abidjan, Ivory Coast, West Africa, one of the most polluted region in the area (Adingra and Kouassi, 2011; Soro et al., 2009). GPS coordinates: Marina Abidjan, Ivory Coast (N 05°20′04.8″/W 004°01′04.9″), Canal Abidjan, Ivory Coast (N 05°20′00.8″/W 004°00′59.2″). Indeed, the pollution type in this area is provided by domestic uses, hospital, cottage industries, etc. Abnormal concentrations of Cu, Zn, Cr and Mn were detected by atomic absorption (Soro et al., 2009). At the same time, an amount of 5 mg L^{-1} of Cu^{II} was added to a water sample extracted from the Touissit river, Morocco (N 34°28′28.3″/W 1°42′58.0″) to check the applicability of the ***SiNNN*** adsorbent in real water doped with copper in North Africa too. An analysis of the composition of these three samples was first carried out to track the eventual presence of alkali and alkaline earth metal cations as well as ammonium (Table 4). As demonstrated in Table 5, the adsorbent shows a high performance in the removal of copper from three samples ~97%, ~95% and ~96% from Marina, Canal and Touissit, respectively.

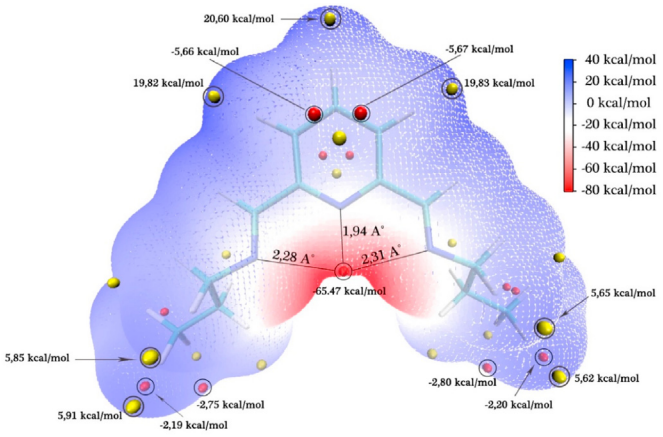

Fig. 10. Analysis of minima and maxima surfaces of molecular electrostatic potential ligand on the surface of silica gel.

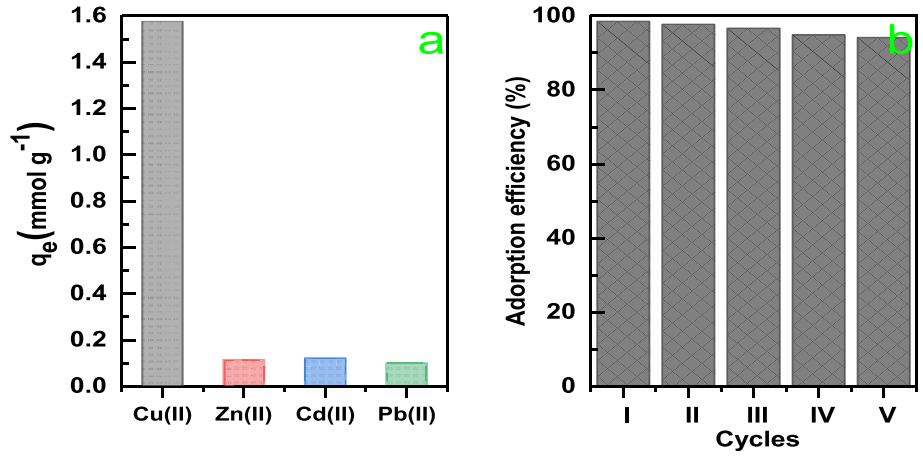

Fig. 9. (a) Metals selectivity effect of ***SiNNN***. (b) five cycles of regeneration using copper adsorption-desorption onto ***SiNNN***.

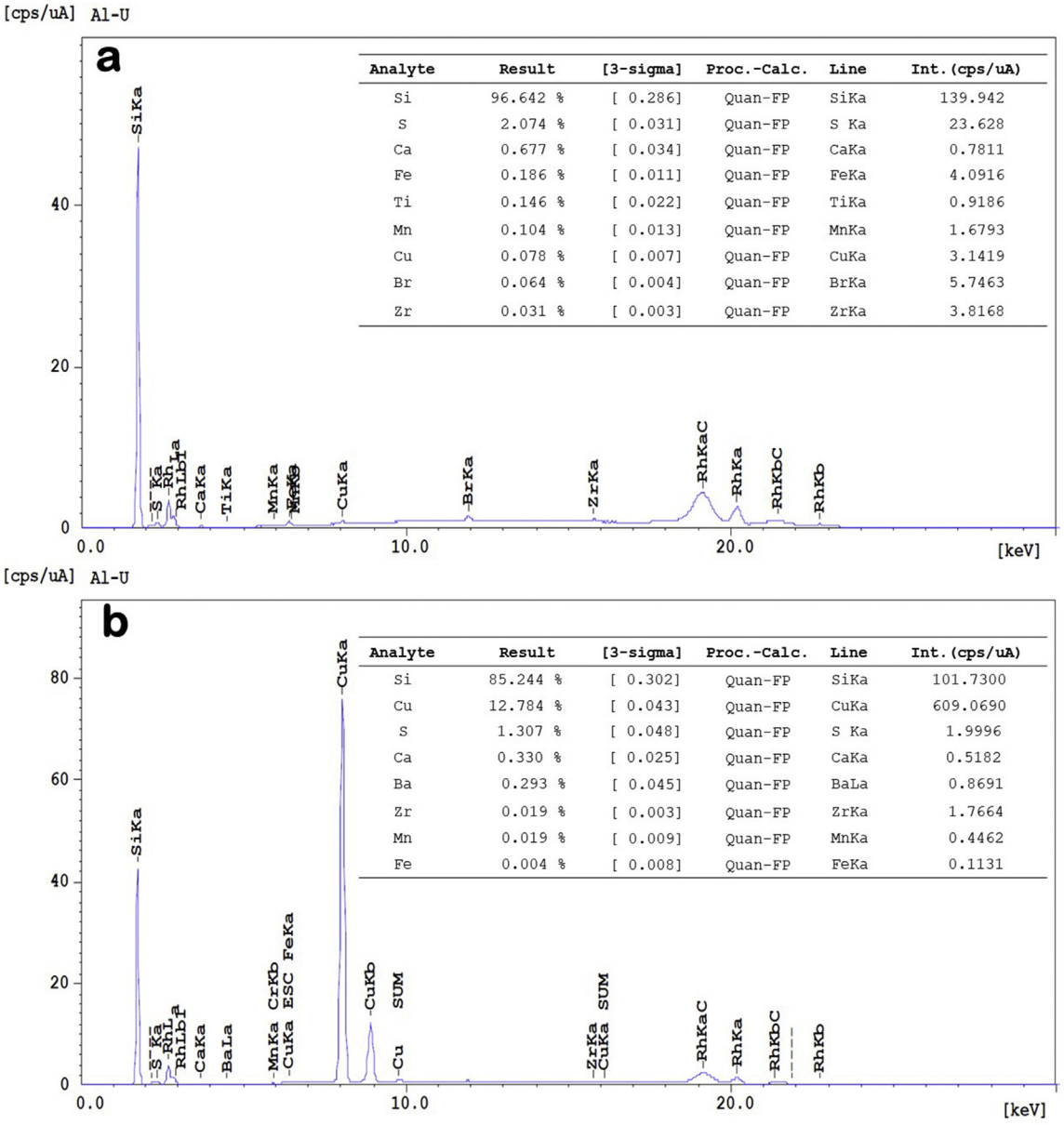

Fig. 11. EDX spectra of adsorbent ***SiNNN*** (a) before and (b) after removal of Cu(II) ions.

Table 4
Cationic ions composition of three real water samples collected in Abidjan and near Oujda.

Cationic Ions	Ca(II) (mmol L^{-1})	Mg(II) (mmol L^{-1})	K(I) (mmol L^{-1})	Na(I) (mmol L^{-1})	NH_4(I) (mmol L^{-1})
Marina	1.242	1.893	0.461	11.292	0.004
Canal	7.214	31.906	6.153	142.515	0.085
Touissit	4.509	5.264	0.111	4.986	0

Table 5
Removal of copper in real wastewater samples from Abidjan and near Oujda. (Conditions: $V = 10$ mL real wastewater sample, $m = 10$ mg of adsorbent, pH = 6, $t = 30$ min, $T = 25$ °C).

Metal ion	Water samples	C_{found} (μmol L^{-1})	Percentage of removal efficiency (%)
Cu(II)	Marina	8.976 ± 0.4	97
	Canal	13.071 ± 0.4	95
	Touissit	76.535 ± 0.4	96

Table 6
Comparison of sorption capacities of adsorbents reported in literature with ***SiNNN***.

Adsorbent sample	Adsorption capacities (mmol g^{-1})				References
	Cu(II)	Zn(II)	Cd(II)	Pb(II)	
This work	1.90	0.52	0.49	0.43	–
Propylamine (***SiNH$_2$***)	0.083	0.12	0.058	0.03	–
N-propyl-2-pyridylimine	0.56	–	–	0.395	Zhang, Y. et al. (2019)
Ethylenediaminepropyl-2-pyridylimine	0.76	–	–	0.514	Zhang, Y. et al. (2019)
Nitrilotriacetic acid	1.00	–	0.47	0.36	Li et al. (2019)
Magnetic polydopamine Nanoparticles	1.36	–	–	0.27	Wang et al. (2018)
3-(2-Aminoethylamino) pro-pyldimethoxymethylsilane	1.17	–	1.08	0.48	Zhu (2015)
Methyl methacrylate	0.65	–	–	–	Mohammadnezhad et al. (2019)
Poly (methyl methacrylate)	1.60	–	–	–	Dinari et al. (2016)
3-hydroxy salicylaldimine propyl triethoxysilane	0.09	–	–	0.01	Koorepazan Moftakhar et al. (2016)
Furan ketonenol	0.50	0.35	0.46	0.09	Radi et al. (2015)
3-amino-1,2-propanediol	0.49	–	–	–	Dong et al. (2018)
Commercial Lewatit (L-207)	1.07	1.11	–	–	Morcali et al. (2014)

Accordingly, ***SiNNN*** material can be applied as a high-performance adsorbent for Cu(II) removal from real aqueous media.

3.2.8. Comparison with other adsorbents

The material ***SiNNN*** is found to be more efficient in the removal of Cu(II), Zn(II), Cd(II) and Pb(II) compared to many adsorbents from the literature (Table 6). As shown in Table 6, the adsorption capacities of the material ***SiNNN*** were higher than that of ***SiNH$_2$***. It is due to the enormous ability to complex metal ions by the ligand on the surface of silica gel.

4. Conclusion

In conclusion, the adsorbent ***SiNNN*** was synthesized via immobilisation of ***PyO*** as ligand on the surface of silica gel, and characterized by several physical methods to investigate the adsorption of trace elements of Cu(II), Zn(II), Cd(II) and Pb(II) ions. The most important adsorption capacity uptake was found for Cu(II) with 1.90 mmol g^{-1} at pH = 6 occurring very quickly (8 min) compared to other metals (20 min) onto ***SiNNN***. The adsorption was found to be endothermic and spontaneous. This material can be reused many times without affecting the adsorption rate. ***SiNNN*** meets practical requirements for complex wastewater containing a variety of organic and metallic contaminants, and can be applied as a high-performance adsorbent for the removal of Cu(II) from real aqueous media, i.e. water samples from the Ebrié Lagoon, one of the most polluted region in Ivory Coast. Research will continue in order to design new adsorbents, extending target metals as well as investigation area in other polluted parts of the world.

CRediT authorship contribution statement

Mohamed El-Massaoudi: Conceptualization, Methodology, Investigation, Data curation, Writing - original draft, Writing - review & editing. **Smaail Radi:** Conceptualization, Supervision, Project administration, Resources, Writing - review & editing. **Morad Lamsayah:** Elaboration of the theoretical part, Data curation, Writing - original draft, Writing - review & editing. **Said Tighadouini:** Experimental part. **Konan Kouakou Séraphin:** Real water sampling, experimental part. **Lazare Kouakou Kouassi:** Supervision, Project administration. **Yann Garcia:** Characterization, Supervision, Writing - review & editing.

Declaration of competing interest

The authors declare that they have no known competing financial interests or personal relationships that could have appeared to influence the work reported in this paper.

Acknowledgements

Wallonie Bruxelles International (WBI−COP22 Morocco) as well as CNRST (ESRSFC-CNRST-P10) are thanked for funding this project. Dr. S. Degoutin and Prof. M. Bacquet (Université de Lille 1, France) are thanked for CHN, ^{13}C NMR, SEM and BET analyses. The Pulse project is also acknowledged in the frame of an Erasmus+KA2 − Capacity Building in the field of Higher Education (CBHE) as well as Prof. J. M. Broto for creating this innovative EU-African network.

References

Abbas, S.H., Ismail, I.M., Mostafa, T.M., Sulaymon, A.H., 2014. Biosorption of heavy metals: a review. J. Chem. Sci. Technol. 3 (4), 74−102.
Abdu, S., Martí-Calatayud, M.-C.s, Wong, J.E., García-Gabaldón, M., Wessling, M., 2014. Layer-by-layer modification of cation exchange membranes controls ion selectivity and water splitting. ACS Appl. Mater. Interfaces 6 (3), 1843−1854.
Adingra, A., Kouassi, A., 2011. Pollution en lagune Ebrié et ses impacts sur l'environnement et les populations riveraines. F. Tech. Doc. Vulg. 48−53.
Al-Saydeh, S.A., El-Naas, M.H., Zaidi, S.J., 2017. Copper removal from industrial wastewater: a comprehensive review. J. Ind. Eng. Chem. 56, 35−44.
Awual, M.R., 2017. New type mesoporous conjugate material for selective optical copper (II) ions monitoring & removal from polluted waters. Chem. Eng. J. 307, 85−94.
Azimi, A., Azari, A., Rezakazemi, M., Ansarpour, M., 2017. Removal of heavy metals from industrial wastewaters: a review. ChemBioEng Rev. 4 (1), 37−59.
Bai, C.-B., Fan, H.-Y., Qiao, R., Wang, S.-N., Wei, B., Meng, Q., Wang, Z.-Q., Liao, J.-X., Zhang, J., Zhang, L., 2019. Synthesis of methionine methyl ester-modified coumarin as the fluorescent-colorimetric chemosensor for selective detection Cu2+ with application in molecular logic gate. Spectrochim. Acta Mol. Biomol. Spectrosc. 216, 45−51.
Barik, B., Kumar, A., Nayak, P.S., Achary, L.S.K., Rout, L., Dash, P., 2020. Ionic liquid assisted mesoporous silica-graphene oxide nanocomposite synthesis and its application for removal of heavy metal ions from water. Mater. Chem. Phys. 239, 122028.
Barrento, S., Marques, A., Teixeira, B., Vaz-Pires, P., Carvalho, M.L., Nunes, M.L., 2008. Essential elements and contaminants in edible tissues of European and American lobsters. Food Chem. 111 (4), 862−867.
Becke, A.D., 1992. Density-functional thermochemistry. I. The effect of the exchange-only gradient correction. J. Chem. Phys. 96 (3), 2155−2160.
Bu, F., Gao, B., Yue, Q., Liu, C., Wang, W., Shen, X., 2019. The combination of coagulation and adsorption for controlling ultra-filtration membrane fouling in water treatment. Water 11 (1), 90.
Burakov, A.E., Galunin, E.V., Burakova, I.V., Kucherova, A.E., Agarwal, S., Tkachev, A.G., Gupta, V.K., 2018. Adsorption of heavy metals on conventional and nanostructured materials for wastewater treatment purposes: a review. Ecotoxicol. Environ. Saf. 148, 702−712.
Chen, K., Zhang, Z., Xia, K., Zhou, X., Guo, Y., Huang, T., 2019. Facile synthesis of thiol-functionalized magnetic activated carbon and application for the removal of mercury (II) from aqueous solution. ACS Omega 4 (5), 8568−8579.
Das, R., Ali, M.E., Hamid, S.B.A., Ramakrishna, S., Chowdhury, Z.Z., 2014. Carbon nanotube membranes for water purification: a bright future in water desalination. Desalination 336, 97−109.

de la Luz-Asunción, M., Pérez-Ramírez, E.E., Martínez-Hernández, A.L., Castano, V.M., Sánchez-Mendieta, V., Velasco-Santos, C., 2019. Non-linear modeling of kinetic and equilibrium data for the adsorption of hexavalent chromium by carbon nanomaterials: dimension and functionalization. Chin. J. Chem. Eng. 27 (4), 912–919.

Dinari, M., Mohammadnezhad, G., Soltani, R., 2016. Fabrication of poly (methyl methacrylate)/silica KIT-6 nanocomposites via in situ polymerization approach and their application for removal of Cu 2+ from aqueous solution. RSC Adv. 6 (14), 11419–11429.

Dong, C., Fu, R., Sun, C., Qu, R., Ji, C., Niu, Y., Zhang, Y., 2018. Comparison studies of adsorption properties for copper ions in fuel ethanol and aqueous solution using silica-gel functionalized with 3-amino-1, 2-propanediol. Fuel 226, 331–337.

El-Massaoudi, M., Radi, S., Bacquet, M., Degoutin, S., Garcia, Y., 2018. Highly efficient and selective adsorbent for potentially toxic metals removal from aquatic media. J. Eniviron. Chem. Eng. 6 (5), 5980–5989.

El Abiad, C., Radi, S., Faustino, M.A., Neves, M., Moura, N.M., 2019. Supramolecular hybrid material based on engineering porphyrin hosts for an efficient elimination of lead (II) from aquatic medium. Molecules 24 (4), 669.

Frisch, M., Trucks, G., Schlegel, H., Scuseria, G., Robb, M., Cheeseman, J., Scalmani, G., Barone, V., Mennucci, B., Petersson, G., 2009. Gaussian09 revision D. 01, Gaussian inc. Wallingford CT. See also. http://www.gaussian.com.

Fu, T., Niu, Y., Zhou, Y., Wang, K., Mu, Q., Qu, R., Chen, H., Yuan, B., Yang, H., 2019. Adsorption of Mn (II) from aqueous solution by silica-gel supported polyamidoamine dendrimers: experimental and DFT study. J. Taiwan Inst. Chem. 97, 189–199.

Gandavadi, D., Sundarrajan, S., Ramakrishna, S., 2019. Bio-based nanofibers involved in wastewater treatment. Macromol. Mater. Eng. 304 (11), 1900345.

Ghosh, M., Layek, M., Fleck, M., Saha, R., Bandyopadhyay, D., 2015. Synthesis, crystal structure and antibacterial activities of mixed ligand copper (II) and cobalt (II) complexes of a NNS Schiff base. Polyhedron 85, 312–319.

Guo, X., Wang, J., 2019. A general kinetic model for adsorption: theoretical analysis and modeling. J. Mol. Liq. 288, 111100.

Gusain, D., Srivastava, V., Sillanpää, M., Sharma, Y.C., 2016. Kinetics and isotherm study on adsorption of chromium on nano crystalline iron oxide/hydroxide: linear and nonlinear analysis of isotherm and kinetic parameters. Res. Chem. Intermed. 42 (9), 7133–7151.

Isasi, J., Arévalo, P., Martin, E., Martín-Hernández, F., 2019. Preparation and study of silica and APTES–silica-modified NiFe 2 O 4 nanocomposites for removal of Cu 2+ and Zn 2+ ions from aqueous solutions. J. Sol. Gel Sci. Technol. 91 (3), 596–610.

Khandaker, S., Toyohara, Y., Saha, G.C., Awual, M.R., Kuba, T., 2020. Development of synthetic zeolites from bio-slag for cesium adsorption: kinetic, isotherm and thermodynamic studies. J. Water Process Eng. 33, 101055.

Koorepazan Moftakhar, M., Dousti, Z., Yaftian, M.R., Ghorbanloo, M., 2016. Investigation of heavy metal ions adsorption behavior of silica-supported Schiff base ligands. Desalin. Water Treat. 57 (56), 27396–27408.

Lee, C., Yang, W., Parr, R.G., 1988. Development of the Colle-Salvetti correlation-energy formula into a functional of the electron density. Phys. Rev. B 37 (2), 785.

Li, Y., He, J., Zhang, K., Liu, T., Hu, Y., Chen, X., Wang, C., Huang, X., Kong, L., Liu, J., 2019. Super rapid removal of copper, cadmium and lead ions from water by NTA-silica gel. RSC Adv. 9 (1), 397–407.

Lu, T., 2014. Multiwfn Software Manual 3.3.6. Beijing Kein Research Center for Natural Sciences, China.

Luque, F.J., López, J.M., Orozco, M., 2000. Perspective on "Electrostatic interactions of a solute with a continuum. A direct utilization of ab initio molecular potentials for the prevision of solvent effects". Theor. Chem. Acc. 103 (3–4), 343–345.

Mohammadnezhad, G., Moshiri, P., Dinari, M., Steiniger, F., 2019. In situ synthesis of nanocomposite materials based on modified-mesoporous silica MCM-41 and methyl methacrylate for copper (II) adsorption from aqueous solution. J. Iran. Chem. Soc. 16 (7), 1491–1500.

Morcali, M.H., Zeytuncu, B., Baysal, A., Akman, S., Yucel, O., 2014. Adsorption of copper and zinc from sulfate media on a commercial sorbent. J. Environ. Chem. Eng. 2 (3), 1655–1662.

Moussout, H., Ahlafi, H., Aazza, M., Maghat, H., 2018. Critical of linear and nonlinear equations of pseudo-first order and pseudo-second order kinetic models. Karbala Int. J. Mod. Sci. 4 (2), 244–254.

Nabeela, Nasreen, S.A.A., Sundarrajan, S., Syed Nizar, S.A., Ramakrishna, S., 2019. Nanomaterials: solutions to water-concomitant challenges. Membranes 9 (3), 40.

Okulik, N., Jubert, A.H., 2005. Theoretical analysis of the reactive sites of non-steroidal anti-inflammatory drugs. Internet Electron. J. Mol. Des. 4 (1), 17–30.

Petrova, P., Karadjova, I., Chochkova, M., Dakova, I., Karadjov, M., 2017. New amino acid modified silica gel sorbents for solid phase extraction of Au (III). Bulg. Chem.Commun. 49, 95–100.

Radi, S., El Abiad, C., Carvalho, A.P., Santos, S.M., Faustino, M.A.F., Neves, M.G.P., Moura, N.M., 2018. An efficient hybrid adsorbent based on silica-supported amino penta-carboxylic acid for water purification. J. Mater. Chem. 6 (27), 13096–13109.

Radi, S., El Abiad, C., Moura, N.M., Faustino, M.A., Neves, M.G.P., 2019. New hybrid adsorbent based on porphyrin functionalized silica for heavy metals removal: synthesis, characterization, isotherms, kinetics and thermodynamics studies. J. Hazard Mater. 370, 80–90.

Radi, S., El Massaoudi, M., Bacquet, M., Degoutin, S., Adarsh, N., Robeyns, K., Garcia, Y., 2017. A novel environment-friendly hybrid material based on a modified silica gel with a bispyrazole derivative for the removal of Zn II, Pb II, Cd II and Cu II traces from aqueous solutions. Inorg. Chem. Front. 4 (11), 1821–1831.

Radi, S., Tighadouini, S., Bacquet, M., Degoutin, S., Janus, L., Mabkhot, Y.N., 2016a. Fabrication and covalent modification of highly chelated hybrid material based on silica-bipyridine framework for efficient adsorption of heavy metals: isotherms, kinetics and thermodynamics studies. RSC Adv. 6 (86), 82505–82514.

Radi, S., Tighadouini, S., El Massaoudi, M., Bacquet, M., Degoutin, S.p, Revel, B., Mabkhot, Y.N., 2015. Thermodynamics and kinetics of heavy metals adsorption on silica particles chemically modified by conjugated β-ketoenol furan. J. Chem. Eng. Data 60 (10), 2915–2925.

Radi, S., Toubi, Y., El-Massaoudi, M., Bacquet, M., Degoutin, S., Mabkhot, Y.N., 2016b. Efficient extraction of heavy metals from aqueous solution by novel hybrid material based on silica particles bearing new Schiff base receptor. J. Mol. Liq. 223, 112–118.

Rasheed, A., Carvalho, A.A.C., de Carvalho, G.G.A., Ghous, T., Nomura, C.S., Esposito, B.P., 2020. Chromium removal from aqueous solutions using new silica gel conjugates of desferrioxamine or diethylenetriaminepentaacetic acid. Environ. Sci. Pollut. Res. 1–10.

Rehman, K., Fatima, F., Waheed, I., Akash, M.S.H., 2018. Prevalence of exposure of heavy metals and their impact on health consequences. J. Cell. Biochem. 119 (1), 157–184.

Römelt, C., Weyhermüller, T., Wieghardt, K.J.C.C.R., 2019. Structural characteristics of redox-active pyridine-1, 6-diimine complexes: Electronic structures and ligand oxidation levels, 380, pp. 287–317.

Dennington, Roy, K, T., Millam, J., 2009. Gaussview, Version 5. Semichem Inc., Shawnee Mission KS.

Salvestrini, S., Leone, V., Iovino, P., Canzano, S., Capasso, S., 2014. Considerations about the correct evaluation of sorption thermodynamic parameters from equilibrium isotherms. J. Chem. Therm. 68, 310–316.

Sarwar, N., Imran, M., Shaheen, M.R., Ishaque, W., Kamran, M.A., Matloob, A., Rehim, A., Hussain, S., 2017. Phytoremediation strategies for soils contaminated with heavy metals: modifications and future perspectives. Chemosphere 171, 710–721.

Scrocco, E., Tomasi, J., 1979. Interpretation by means of electrostatic molecular potentials. Adv. Quant. Chem. 11, 115.

Song, X., Niu, Y., Zhang, P., Zhang, C., Zhang, Z., Zhu, Y., Qu, R., 2017. Removal of Co (II) from fuel ethanol by silica-gel supported PAMAM dendrimers: combined experimental and theoretical study. Fuel 199, 91–101.

Soro, G., Métongo, B., Soro, N., Ahoussi, E., Kouamé, F., Zade, S., Soro, T., 2009. Heavy metals (Cu, Cr, Mn and Zn) in surface sediments from a tropical african lagoon: case of the Ebrie lagoon (Ivory coast). Int. J. Biol. Chem. Sci. 3 (6), 1408–1427 (in French).

Sosa, N., Chanlek, N., Wittayakun, J., 2020. Facile ultrasound-assisted grafting of silica gel by aminopropyltriethoxysilane for aldol condensation of furfural and acetone. Ultrason. Sonochem. 62, 104857.

Tighadouini, S., Radi, S., Anannaz, M., Bacquet, M., Degoutin, S., Tillard, M., Eddike, D., Amhamdi, H., Garcia, Y., 2018. Engineering β-ketoenol structure functionality in hybrid silica as excellent adsorbent material for removal of heavy metals from water. New J. Chem. 42 (16), 13229–13240.

Tighadouini, S., Radi, S., Bacquet, M., Degoutin, S., Zaghrioui, M., Jodeh, S., Warad, I., 2017. Removal efficiency of Pb (II), Zn (II), Cd (II) and Cu (II) from aqueous solution and natural water by ketoenol–pyrazole receptor functionalized silica hybrid adsorbent. Separ. Sci. Technol. 52 (4), 608–621.

Tighadouini, S., Radi, S., Elidrissi, A., Zaghrioui, M., Garcia, Y., 2019. Selective confinement of CdII in silica particles functionalized with β-keto-enol-bisfuran receptor: isotherms, kinetic and thermodynamic studies. Eur. J. Inorg. Chem. 2019 (27), 3180–3186.

Tighadouini, S., Radi, S., Garcia, Y., 2020. Selective chemical adsorption of Cd (ii) on silica covalently decorated with a β-ketoenol-thiophene-furan receptor. Mol. Syst. Des. 5, 1037–1047.

Vojoudi, H., Badiei, A., Amiri, A., Banaei, A., Ziarani, G., Schenk-Joß, K., 2018. Preconcentration of Zn (II) ions from aqueous solutions using meso-porous pyridine-enrobed magnetite nanostructures. Food Chem. 257, 189–195.

Wang, N., Yang, D., Wang, X., Yu, S., Wang, H., Wen, T., Song, G., Yu, Z., Wang, X., 2018. Highly efficient Pb (ii) and Cu (ii) removal using hollow Fe 3 O 4@ PDA nanoparticles with excellent application capability and reusability. Inorg. Chem. Front. 5 (9), 2174–2182.

Weitzer, M., Brooker, S., 2005. Dimetallic complexes of a structurally versatile pyridazine-containing Schiff-base macrocyclic ligand with pendant pyridine arms. Dalton Trans. 2448–2454.

Wondracek, M.H.P., Jorgetto, A.O., Silva, A.C.P., do Rocio Ivassechen, J., Schneider, J.F., Saeki, M.J., Pedrosa, V.A., Yoshito, W.K., Colauto, F., Ortiz, W.A., 2016. Synthesis of mesoporous silica-coated magnetic nanoparticles modified with 4-amino-3-hydrazino-5-mercapto-1, 2, 4-triazole and its application as Cu (II) adsorbent from aqueous samples. Appl. Surf. Sci. 367, 533–541.

Xu, Z., Wang, K., Liu, Q., Guo, F., Xiong, Z., Li, Y., Wang, Q., 2018. A bifunctional adsorbent of silica gel-immobilized Schiff base derivative for simultaneous and selective adsorption of Cu (II) and SO42−. Separ. Purif. Technol. 191, 61–74.

Zhang, P., Niu, Y., Qiao, W., Xue, Z., Bai, L., Chen, H., 2018. Experimental and DFT investigation on the adsorption mechanism of silica gel supported sulfur-capped PAMAM dendrimers for Ag (I). J. Mol. Liq. 263, 390–398.

Zhang, W., Zhang, Y., Zhang, Y., Lan, C., Miao, Y., Deng, Z., Ba, X., Zhao, W., Zhang, S., 2019a. Tetra-proline modified calix [4] arene bonded silica gel: a novel stationary phase for hydrophilic interaction liquid chromatography. Talanta 193,

56–63.
Zhang, Y., Cao, X., Sun, J., Wu, G., Wang, J., Zhang, D., 2019b. Synthesis of pyridyl Schiff base functionalized SBA-15 mesoporous silica for the removal of Cu (II) and Pb (II) from aqueous solution. Journal of Sol-Gel Science Technology, 1–13.
Zhao, J., Luan, L., Li, Z., Duan, Z., Li, Y., Zheng, S., Xue, Z., Xu, W., Niu, Y., 2020. The adsorption property and mechanism for Hg (II) and Ag (I) by Schiff base functionalized magnetic Fe3O4 from aqueous solution. J. Alloys Compd. 825, 154051.
Zhou, X., Zhou, X., 2014. The unit problem in the thermodynamic calculation of adsorption using the Langmuir equation. Chem. Eng. Commun. 201 (11), 1459–1467.
Zhu, Z., 2015. Preparation and characterization of functionalized silica spheres for removal of Cu (II), Pb (II), Cr (VI) and Cd (II) from aqueous solutions. RSC Adv. 5 (36), 28624–28632.